Proceedings of ASME Turbo Expo 2011
GT2011
June 6-10, 2011, Vancouver, British Columbia, Canada

GT2011-45246

INTERACTION OF VORTEX SHEDDING AND TRANSVERSE HIGH-FREQUENCY PRESSURE OSCILLATIONS IN A TUBULAR COMBUSTION CHAMBER

Joachim Schwing[*]**, Thomas Sattelmayer**
Lehrstuhl für Thermodynamik
TU München
Garching, Germany
Email: schwing@td.mw.tum.de

Nicolas Noiray
ALSTOM Power
Baden, Switzerland

ABSTRACT

Intense research on the thermoacoustic stability of premixed gas turbine combustors in the past two decades has led to an improved understanding of instabilities of longitudinal modes in the sub-kHz range and predictive tools for thermoacoustic stability analysis have also been developed. Circumferential modes in annular combustors have been studied in the past as well, even though to a much lower extent due to the high experimental effort. Combined experimental-numerical methods for the low-frequency regime (i.e. acoustically compact flames) are widely used. However, such experimental and numerical approaches with predictive capability have to be developed to also address the high-frequency (HF) regime. An experimental study of HF thermoacoustic coupling is presented in this paper. A fully premixed swirl-stabilized flame at atmospheric condition in a cylindrical combustion chamber is investigated. The test rig is equipped with several dynamic pressure transducers to identify and reconstruct the acoustic field in the combustion chamber. Planar information about the flame front location is obtained from Mie-scattering and the flow field is measured with particle image velocimetry (PIV). In the tests the first transverse mode of the combustion chamber exhibits instability for a particular operating condition, which leads to sustained limit-cycle pulsations. Mie-scattering images reveal periodic vortex shedding at the outlet of the burner. PIV results provide quantitative information on the strength of these coherent shear layer vortices.

[*]Address all correspondence to this author.

Keywords: *Thermoacoustics, high-frequency instabilities, transverse mode.*

NOMENCLATURE

a Speed of sound
f Frequency
p Acoustic pressure
x Horizontal/burner axis
y Vertical axis
z Horizontal axis
D Diameter of flame tube

INTRODUCTION

With the introduction of premixed combustion in gas turbines several decades ago, thermoacoustic instabilities have become increasingly problematic. A wide range of methods for the prediction of such instabilities have been developed, which provide adequate methods for the description of wave propagation and thermoacoustic feedback [1]. Due to the yet unresolved problem of deriving the flame response with sufficient precision from theory or computational fluid dynamics these tools are mostly combined experimental-numerical approaches [2, 3] assuming compact flames. However, these approaches based on transfer function models are restricted to low frequencies, i.e. only applicable if the acoustic wavelength is much larger than flame size. While numerous studies dealing with compact flame combustion instabilities can be found in the literature, much less experimental work has been reported in the literature concerned with HF-instabilities of premixed turbulent swirl flames.

Paschereit et al. [4] investigated high-frequency instabilities when using partially premixed-diffusion flames in swirl-stabilized combustors. The influence of transverse acoustic excitation on annular jets is shown by O'Connor et al. [5]. Huang et al. [6] and Huang and Yang [7] studied unsteady flow motions in swirl-stabilized combustion and identified helical vortex structures and transverse pressure oscillations in their numerical work.

The physical phenomena of unstable shear layers was investigated for the first time in history by Thomson (Lord Kelvin) [8] and Helmholtz [9]. Even though the work of Kelvin and Helmholtz is based on a much simpler configuration, similar observations were made – among others – in above-mentioned literature in swirl-stabilized flames. Perturbations of the shear layer are convectively unstable. The perturbations grow, roll up and form vortices.

The goal of this work is to present a well controlled experimental setup exhibiting a HF instability of a fully premixed swirl-stabilized turbulent flame in a cylindrical chamber, and to extract from combined acoustic-PIV measurements the driving mechanism leading to a strong self-sustained first tangential eigenmode. The test rig is presented in the first section, followed by the description of the measurement techniques used to investigate the combustion instability. Experimental results are then analyzed and a feedback mechanism is proposed in the last section.

EXPERIMENTAL SETUP

The experiments presented in the paper were made in a single burner test rig. The plenum of the test rig is fed with the preheated and premixing fuel air mixture. The fuel is injected into the air in a prechamber. The injection holes are spread around multiple positions in the prechamber. The prechamber is connected to the plenum by a static mixer to ensure a homogeneous mixture of fuel and air. The swirler is mounted in the plenum and a mixing tube is mounted at its exit. At the downstream end of the mixing tube at the transition to the combustor the flow cross section changes abruptly in order to generate breakdown of the swirling flow, which is required for the stabilization of flames in swirl burners without centerbody. The plate between mixing tube and combustion chamber is subsequently called front plate, also known as dump plate in literature. The flow transition leads to the typical recirculation zone in the center of the flow. A cylindrical flame tube is used as combustion chamber, which results in simple acoustic mode shapes. The diameter of the flame tube is $D = 156$ mm. The exhaust cooling, directly attached to the flame tube, has the same diameter as the flame tube. Flame tube plus exhaust cooling pipe are approximately 2 m long before dumping the flow. The test rig is shown in Fig. 1. The mean flow is

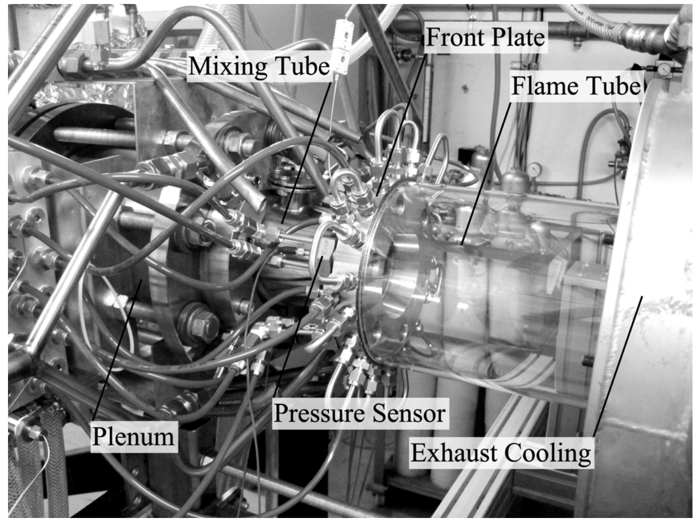

FIGURE 1. Setup of test rig with (from left to right) plenum, mixing tube, front plate, flame tube, and exhaust gas cooling.

directed from left to right. The plenum is to the left of the image, followed by mixing tube, front plate, flame tube, and exhaust gas cooler. The flame tube is manufactured in quartz glass. The front plate is water-cooled and can be equipped with up to six dynamic pressure sensors at its circumference. More information on the test rig and the burner are presented in [10]. An analysis of the mean flow field and of OH* chemiluminescence images can be found there as well.

Dynamic pressure measurements

The dynamic pressure sensors are of type PCB 106B/064B06. The front plate and the five piezoelectric sensors are water-cooled. The sensors are flush-mounted to the front plate facing the flame. The probe volumes are located on a circle with the diameter $d = 124$ mm in the y-z-plane at $x = 0$, when referring to the cartesian coordinate system in Fig. 2. Looking in mean flow direction, i.e. in x-direction, the sensors are mounted in the front plate at 2, 4, 6, 8, and 10 o'clock position (60, 120, 180, 240, 300 degrees). Subsequently we refer to the sensors as 'Sensor 60,' 'Sensor 120,' etc. Looking through the quartz glass into the flame tube in Fig. 1 the front of the sensors in the flame tube is visible. As all sensors are located on the front plate, the longitudinal amplitude decay of the excited first transverse eigenmode cannot be retrieved with the current setup.

Optical measuring techniques

Besides acoustic measurements, optical techniques are used to get information on the flow field and on the turbulent flame. The flow is seeded with titanium dioxide particles. The beam

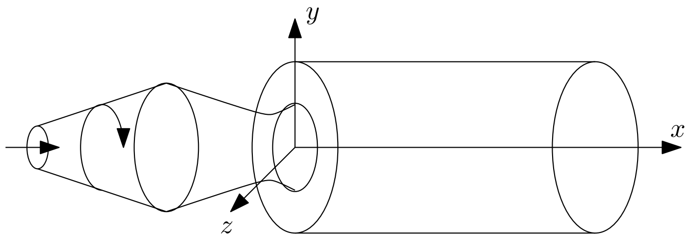

FIGURE 2. Sketch of test rig showing swirler, mixing tube, and flame tube (from left to right) with cartesian coordinate system in flame tube.

of a laser with two cavities operated at 10 kHz is widened to a laser sheet, illuminating a single plane – the *x*-*y*-plane – in the combustion chamber. The scattering image is recorded by a high-speed camera. The optical axis of the camera is parallel to the *z*-axis.

Mie-scattering images are recorded at 20 kHz and used to extract density information and to differentiate between unburnt mixture of fuel and air and combustion products. For more background information on this technique the reader is referred to Gülder et al. [11] or Pfadler et al. [12].

Local flow velocities are measured by using particle image velocimetry (PIV). The repetition rate of PIV is limited to 10 kHz. Fig. 3 shows the test rig equipped with the optical instrumentation. The high-speed camera is visible in the back behind the quartz tube. On the top right the optics of the laser system is apparent. The laser sheet is applied from top through the burner axis. The optics is inclined, the laser beams are not perpendicular to the surface of the quartz tube, to avoid reflections and refractions in the quartz glass tube. This is not necessary for pure Mie-scattering images, but improves signal quality of detailed PIV measurements. ‘Sensor 60’ is used as reference. To avoid titanium dioxide particles entering and destroying the sensor, it is permanently purged with a flow of air.

OH* chemiluminescence

OH* chemiluminescence is used as an indicator for heat release [13]. The OH* signal of the flame is recorded with a photomultiplier tube (PMT). The light is filtered by a narrowband optical filter at a wavelength of 307 nm. The optical setup in front of the PMT consists of multiple lenses and apertures to create a narrow viewing angle [14]. The observed volume in the flame corresponds to a cylinder with a diameter of 2 to 3 mm. Thus the recorded signal is an integral value. The signal is used to identify high-frequency fluctuations and to compare the mean intensity and the intensity of fluctuations at multiple positions. The PMT is mounted similar to the high-speed camera in Fig. 3. The axis of the cylindrical recording volume is parallel to the *z*-axis. The horizontal (*x*-axis) and vertical (*y*-axis) position is varied. When correlating the OH* chemiluminescence to pressure, the Rayleigh criterion can be evaluated and the feedback

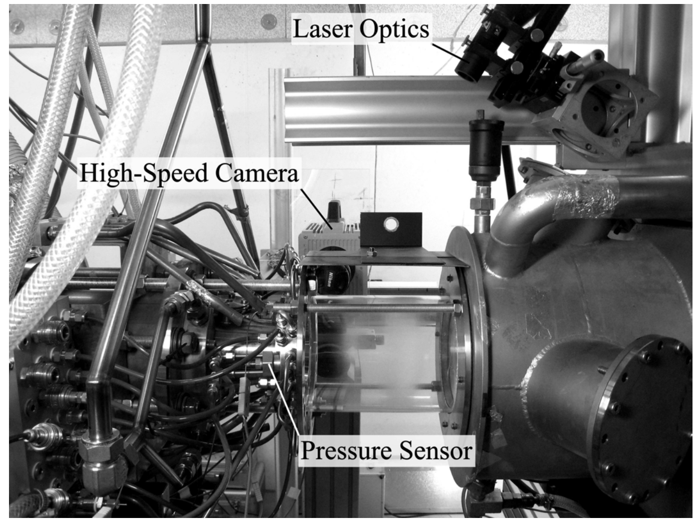

FIGURE 3. Setup of laser measuring technique with high-speed camera (behind quartz tube), laser optics (top right), and air purged reference pressure sensor (front of quartz tube).

of acoustics and heat release can be characterized [15, 16]. For detailed analysis of mean OH* chemiluminescence intensity and flame length it is referred to [10].

RESULTS AND DISCUSSION

The results presented in the following are obtained with the test rig being operated at one single operating point. Air and fuel are preheated to 300 °C. Natural gas is used as fuel. The equivalence ratio of the mixture is one, thus the burner is operated at stoichiometric conditions. The mass flow rate of air is set to 80 g/s.

Changing the mass flow rate or the inlet temperature, self-excited instabilities are observed at slightly different stoichiometric ratios and frequencies. However, a detailed analysis of different settings is not part of this study. It seems to be more sophisticated to the authors to analyze the feedback mechanism first and transfer the knowledge to different operating conditions later.

Pressure measurements

The Fourier spectrum of the pressure signal recorded by ‘Sensor 60’ is shown in Fig. 4. The amplitude measured in dB (SPL) is plotted as a function of the frequency. The plot of the other four sensors is very similar and is thus omitted. The sixth sensor position is occupied by a dummy equipped with thermocouples to measure the operating temperature of the sensors. All five sensors clearly indicate a peak at 3.3 kHz. Harmonics are observed and most probably result from nonlinear acoustic wave propagation [17].

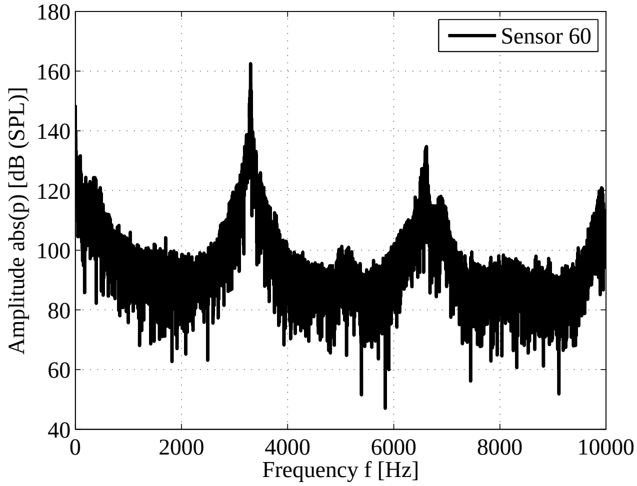

FIGURE 4. Pressure amplitude as a function of frequency showing a peak at 3.3 kHz.

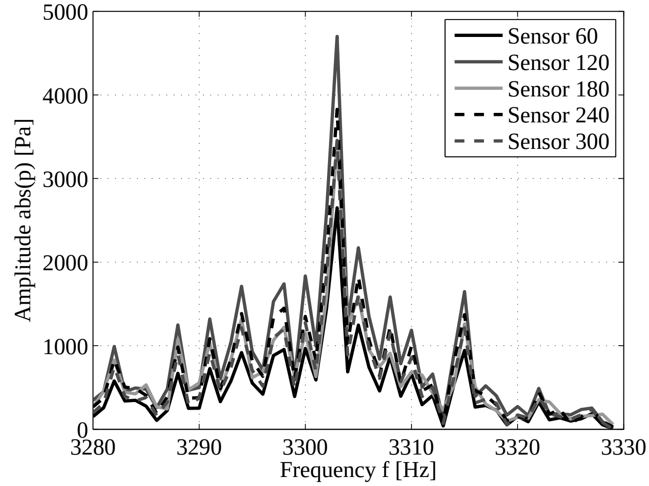

FIGURE 5. Pressure amplitude around the peak at 3.3 kHz.

Fig. 5 gives a closer look at the peak frequency and the secondary peaks, which are present in a ± 15 Hz range. These peaks result from a low frequency modulation of the limit cycle amplitude. The amplitude is plotted in Pascal. The authors would like to recall here, that a low-frequency modulation of the limit cycle amplitude with the frequency f_a is different from a low-frequency oscillation at the frequency f_a. The fourier transform of a low-frequency oscillation results in a peak at the frequency f_a, where the modulation of the limit cycle amplitude results in secondary peaks at $f - f_a$ and $f + f_a$ – besides a larger peak at the frequency f.

Back to Fig. 5, 'Sensor 60' and 'Sensor 120' deviate in their maximum amplitude from the other sensors. This deviation is reproducible if using the same physical sensor at the same physical position. From interchanging sensors it can be concluded that the sensors show different temperature sensitivity, but the sensor amplitudes were only calibrated at ambient temperature. Exact calibration of the amplitude at high temperature is postponed as phase information is more important in this context which does not depend on the sensor's temperature.

Fig. 6 depicts the phase angle of the pressure signals taking 'Sensor 60' as a reference. The frequency range on the *x*-axis is identical to Fig. 5. The amplitude is represented by the grayscale, black denotes maximum amplitude and white zero amplitude. The phase difference between opposing sensors, 'Sensor 60' and 'Sensor 240' or 'Sensor 120' and 'Sensor 300', is 180 degrees indicating a first transverse mode, referred to as T1 mode in the following. The eigenfrequency of a T1 mode in a circular cylinder can be estimated to

$$f_{T1} = \frac{\alpha_{T1} a}{2\pi R} = 3305\ \text{Hz}, \tag{1}$$

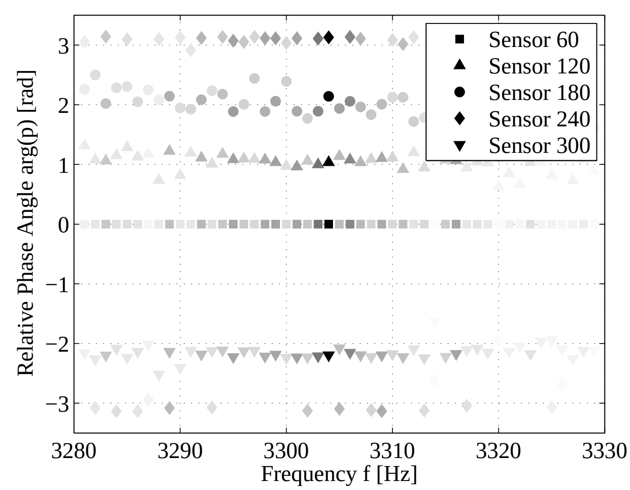

FIGURE 6. Phase angle around 3.3 kHz with maximum amplitude in black and zero amplitude in white.

where $\alpha_{T1} = 1.841$ is the characteristic value of the Bessel function of the T1 mode, $a = 880$ m/s is an estimate for the speed of sound in the exhaust gas at a temperature of 2000 K, and $R = 78$ mm denotes the radius of the cylindrical flame tube [18]. The value for the exhaust gas temperature results from a qualified guess of the heat losses in the system but is not measured. Thus f_{T1} has to be considered as a rough estimate itself. On the other hand the frequency f_{T1} is only the cut-on frequency of the T1 mode. At freqencies $f > f_{T1}$ a mixed transverse-longitudinal mode can establish in the chamber. Mixed modes are transverse modes with a longitudinal component. Due to the current configuration of the test rig the longitudinal wave length cannot be

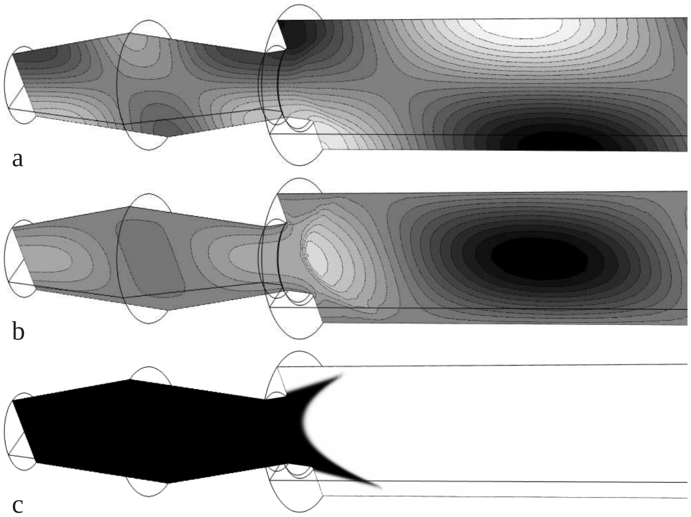

FIGURE 7. Acoustic pressure (a), y-component of the acoustic velocity (b) of a T1 mode in combustor with temperature profile (c) in x-y-plane. Minimum is marked black, maximum white. Pressure and velocity are shifted by $\pi/2$.

identified in the experiments.

But calculations from the design phase of the experiments illustrate mixed modes, see Fig. 7. The acoustic pressure in the x-y-plane is shown in Fig. 7 (a). Positive pressure amplitude is marked white, negative amplitude black. On the nodal lines, e.g. the x-axis, the amplitude of the acoustic pressure is zero. The acoustic y-velocity fluctuation is presented in Fig. 7 (b). The plot of the velocity fluctuation is phase shifted by $\pi/2$ compared to the pressure field, as the velocity fluctuations are zero at maximum pressure and acoustic pressure is zero if the velocity fluctuations are maximum. White denotes a positive y-velocity and black a negative one. The presumed axisymmetric temperature profile is depicted in Fig. 7 (c). Mean flow effects are neglected when solving the time-harmonic formulation of the linearized Euler equations.

Back to the experiments, the phase difference between neighboring sensors in Fig. 6, which are spaced at a geometric angle of 60 degrees, is 60 degrees and independent of frequency. This means, that the T1 mode is a single rotating transverse mode and the angular frequency of the rotation is identical to the frequency of the pressure oscillation, i.e. 3.3 kHz. If the transverse mode was a stationary and not a rotating mode, the plot, c.p. Fig. 6, would only show phase lags of 0 and π. From the sign of the phase difference in Fig. 6 it can be concluded, that the mode is rotating counterclockwise if looking in mean flow direction. Direction of swirl and rotational direction of the acoustic mode are identical.

The rotating nature of the mode is a first indicator – but not a proof – that the thermoacoustic coupling/damping is uniform along the circumference, which was expected with such pure symmetric geometry. Noiray et. al. [19] showed analytically, that acoustic modes do not lock spatially, if the coherent heat release response strength does not depend on the azimuth.

Summarizing above observations, measurements of the dynamic pressure show the existence of a self-excited counterclockwise rotating T1 mode in the flame tube.

Mie-scattering

The analysis of the Mie-scattering images is used to locate unburnt and burnt mixture at a high repetition rate of 20 kHz resolving all phenomena at the acoustic peak frequency of 3.3 kHz. Fig. 8 shows a single snapshot of the entire combustion chamber. The bright horizontal lines are caused by reflections of the laser sheet in the quartz glass tube. The mean flow is from left to right. Unburnt gas, i.e. premixed air and fuel, is depicted white and combustion products appear gray to black. The density of unburnt gas is high, thus the amount of titanium dioxide seeding per volume is large, which in turn leads to intense Mie-scattering. Combustion products have a high temperature and a low density, thus the amount of seeding particles per volume is low and the intensity of scattered light is reduced compared to unburnt gas [11, 12].

Fig. 8 clearly indicates periodic structures of recirculated combustion products (black) in the unburnt mixture of air and fuel (white). The recirculation zones in the upper and the lower half are in phase opposition, similar to the acoustics of the T1 mode in the considered plane, c.p. Fig. 7. The white square in the image highlights the close-up view subsequently analyzed in greater depth.

Fig. 9 shows a series of six Mie-scattering images equally spaced throughout a complete 3.3 kHz cycle. Next to each scattering image we show the reconstructed pressure signal in the observed area at the front plate. The pressure field at the front plate is reconstructed via the recording of the reference sensor knowing the mode shape, rotation, etc. The signal of the reference sensor is Fourier transformed and decomposed into amplitude and phase. The phase is shifted according to the geometric angle, the amplitude is kept constant as the radius of the recorded position is already correct. The modified phase is then combined with the amplitude, obtaining the time trace of the pressure signal when applying the inverse Fourier transform. The reconstruction was validated with the signal at different positions when using no seeding in the flow.

The current pressure value in Fig. 9 is indicated with a circle. The white line to the left of each scattering image results from the light scattered by the front plate and it can be used as a reference to locate the shear layer position with respect to the mixing tube outlet. The lower left triangle of the images is almost dark, because this part is not directly illuminated by the

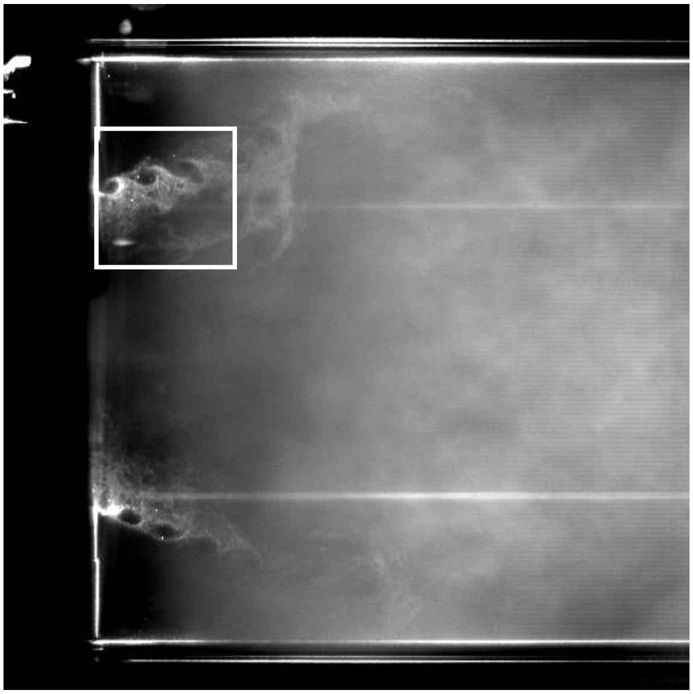

FIGURE 8. Mie-scattering image of complete flame tube.

laser sheet to avoid reflections from the quartz tube.

The observations made in the scattering images concentrate on the upper shear layer, i.e. the layer between unburnt gas and combustion products in the outer recirculation zone. The position of the shear layer close to the front plate oscillates in phase with the pressure. At maximum pressure it is at its maximum radius (high up in Fig. 9 (a)), at minimum pressure it is located at its minimum radial position (far down in Fig. 9 (d)). During the transition from minimum to maximum pressure (Fig. 9 (e) and (f)), combustion products are engulfed in the moving unburnt mixture at the front plate. Subsequently, the engulfed recirculated combustion products are convectively transported with the mean flow. In the first three images (Fig. 9 (a) to (c)) it is apparent that the engulfed combustion products separate from the front plate. In the last image (Fig. 9 (f)) the next recirculated combustion product zone is generated with increasing pressure.

From the Mie-scattering images we conclude, that combustion products are periodically engulfed by the unburnt mixture of fuel and air. This happens at the outer shear layer of the swirl flow, where the unburnt mixture enters the combustion chamber. The pocket of combustion products is then convected downstream by the mean flow. No coherent structures were observed at the inner shear layer of the swirl flow, the shear layer between unburnt mixture and the inner recirculation zone.

Particle image velocimetry

PIV measurements were done to clarify the nature of the pocket of combustion products and to investigate the interaction of acoustics and flow at the front plate. For mean velocity fields it is referred to [10]. The plots in Fig. 11 depict a series of three successive shots. It is obvious, that three vector fields per cycle are not sufficient to completely resolve the observed phenomena. However, the repetition rate is limited by the available hardware. Thus the conclusions are drawn from multiple shots, but for convenience only one cyle is presented. The recorded vector fields (Fig. 11) show in detail the interaction of acoustic velocity, unburnt mixture, and outer recirculation zone, in particular the separation of the recirculated, engulfed combustion products at the front plate. The zones of reciculated combustion products are clearly identified as vortices. The vortices are convectively transported as exposed to a mean flow. Please note that Fig. 11 shows absolute velocity vectors and the center of a vortex has only zero velocity in the relative frame.

The velocity vectors in Fig. 11 (a) are mainly directed upwards, in particular in the outer recirculation zone (top half). In general one would expect a velocity component downwards in the outer recirculation zone. In the unburnt mixture (lower half) the mean flow still dominates, but – in particular when comparing to the subsequent subfigures – the upward tendency is apparent. From pressure measurements it can be concluded that Fig. 11 (a) corresponds Fig. 9 (f). The acoustic pressure is close to zero, the acoustic velocity is at its maximum amplitude and directed upwards. As velocity vectors in the recirculation zone are directed upwards, the acoustic velocity dominates over the flow of the outer recirculation zone.

At the corner of the front plate, where unburnt mixture enters the flame tube, the flow velocity of the unburnt mixture is very high. Thus the acoustic velocity is not able to force the flow to attach to the front plate directly. A zone of recirculated combustion products remains at the corner and is surrounded by unburnt gas, which attaches to the front plate further up. An engulfed region of combustion products is generated and forced to rotate by the passing unburnt gas, thus a vortex is formed. Fig. 10 illustrates the process leading to zones of engulfed combustion products. The arrow marked with the character ‘a’ visualizes the deflection of streamlines, whereas combustion products remain at the front plate.

In Fig. 11 (b) the formation of a vortex at the front plate is apparent. This step corresponds to Fig. 9 (b). The sign of the acoustic velocity has turned. The acoustic velocity is directed downwards. A zone of recirculated combustion products has separated from the outer recirculation zone. This is illustrated by the arrow ‘b’ in Fig. 10.

Fig. 11 (c) corresponds to Fig. 9 (d). The vortex was forced downwards and is convected with the mean flow. The acoustic velocity is close to zero as the pressure is at one of its extrema. As the velocity field is not superimposed by the acoustic veloc-

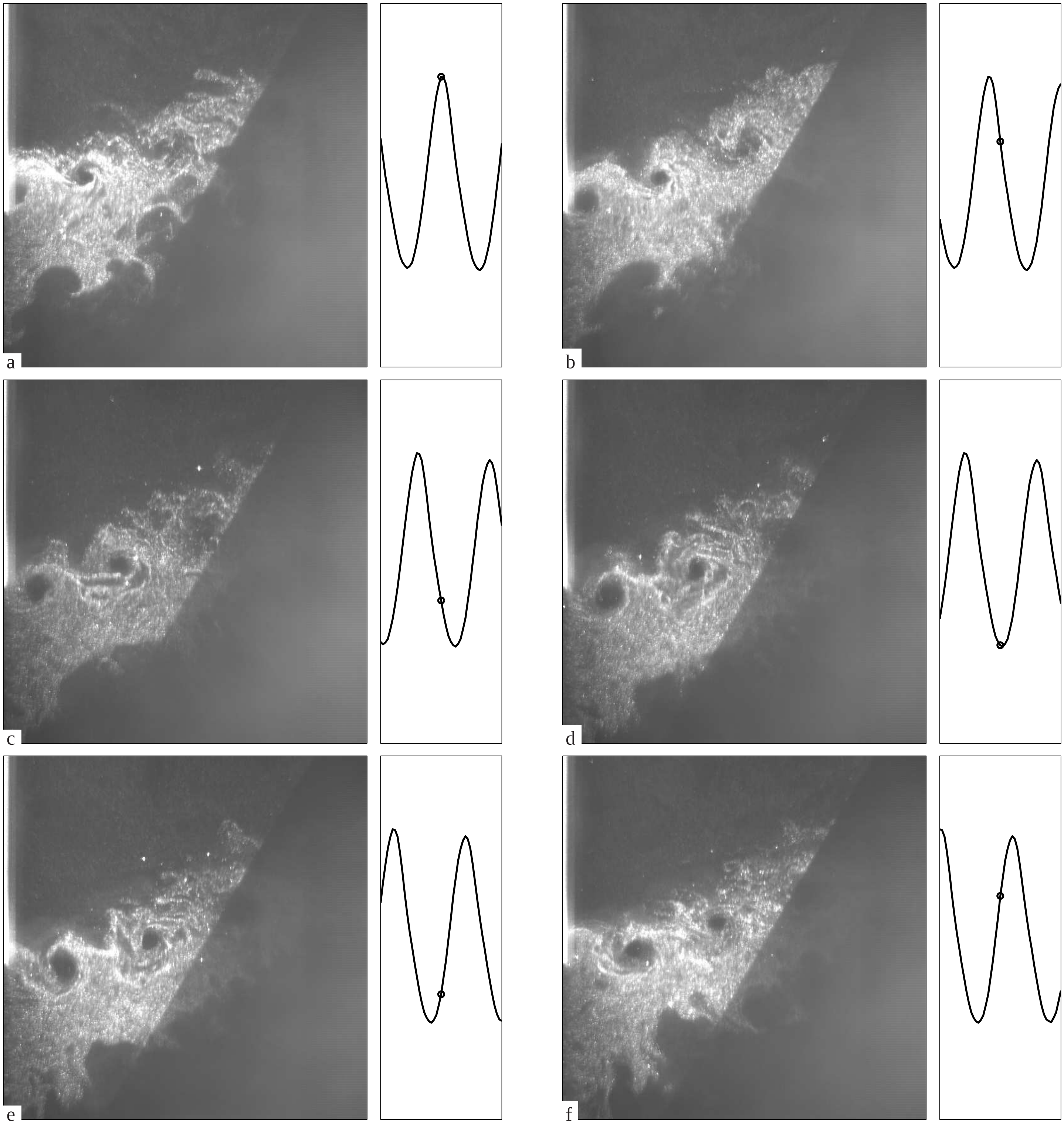

FIGURE 9. Mie-scattering images compared to high-frequency pressure oscillations.

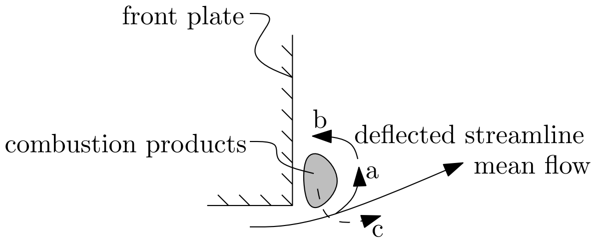

FIGURE 10. Sketch of interaction of flow and acoustics leading to the formation of engulfed combustion products and vortices.

ity in Fig. 11 (c), the flow field in the outer recirculation zone and around the vortices is evident. This step is illustrated by the arrow ‘c’ in Fig. 10.

In summary, PIV and Mie-scattering indicate clearly, that the vortices are generated by the interaction of the acoustic velocity and the mean flow at the corner of the front plate, where unburnt mixture enters the flame tube. The acoustic velocity triggers this phenomenon. The vortices with engulfed combustion products are convectively transported with the unburnt mixture. Due to the limitations by the available hardware it was not possible to obtain a higher temporal resolution of the phenomenon. Phase locked measurements could compensate for a low repetition rate. As the position of the outer shear layer varies due to turbulence, the exact position of the vortices is not constant all the time but stochastically distributed. Thus the evaluation of phase locked data is very costly and hard to interpret.

OH* chemiluminescence

As mentioned above, OH* chemiluminescence of the flame is used as an indicator for heat release here. Planar laser-induced fluorescence (PLIF) of OH would be favorable, but will only be realized in the future. Fig. 12 shows the recorded signal at multiple positions. The horizontal axis x is parallel to the burner axis and the y-axis is perpendicular to it, c.p. Fig. 2. The origin of the coordinate system is in the center of the tubular quartz glass combustion chamber at the inlet plane. The intensities are normalized, the mean values to the maximum measured mean value and the fluctuating OH* values to the maximum amplitude of the fluctuations around 3.3 kHz. The maximum value or amplitude is drawn in black. No intensity is represented by white.

Mean intensities (squares) are zero in the outer shear layer, e.g. at $x = 15$ mm and $y > 45$ mm. In the inner shear layer mean intensities are significantly larger, see $x = 15$ mm and $y < 45$ mm. Due to line-of-sight integration mean intensities do not vanish at the axis of the flame, i.e. $y = 0$ mm. Fluctuations around the frequency of 3.3 kHz (bullets) peak in the inner shear layer. The maximum intensity of fluctuations are observed near $x = 25$ mm and $y = 40$ mm. The intensity of the fluctuation is approximately 15 percent of the mean amplitude there. At the

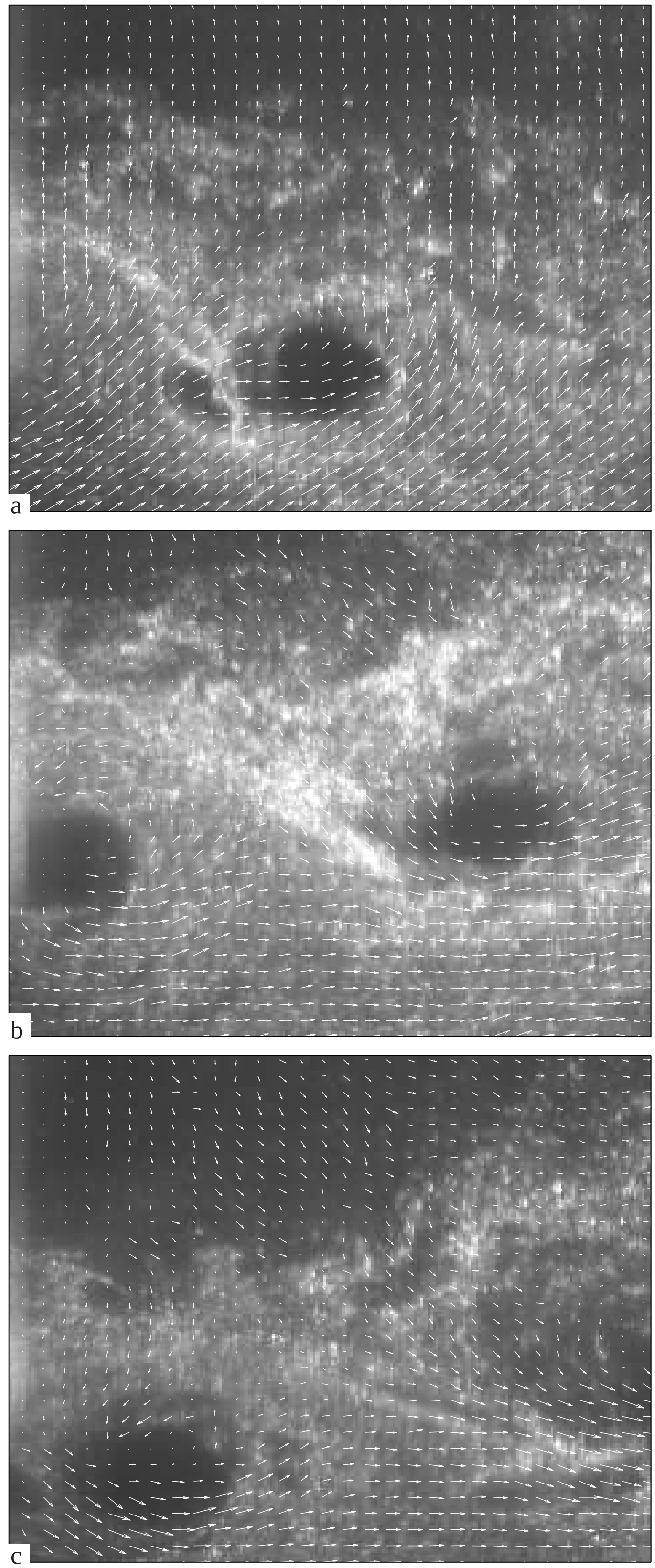

FIGURE 11. Flow field measured by PIV.

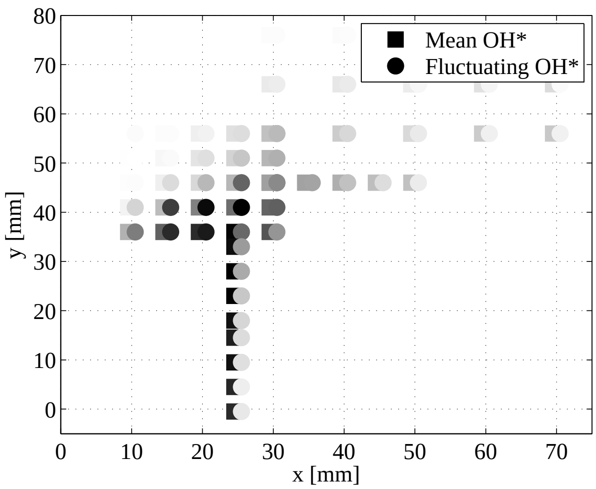

FIGURE 12. Intensity of mean and fluctuating OH* chemiluminescence recorded with photomultiplier using optics with narrow viewing angle. Grayscale from no intesity (white) to maximum value/amplitude (black).

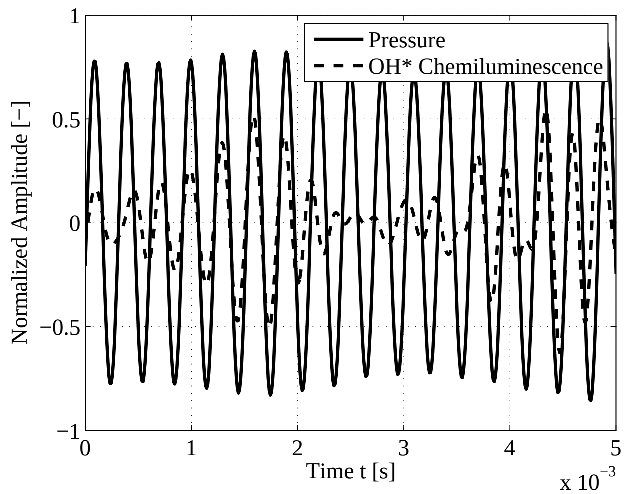

FIGURE 13. Bandpass filtered pressure and OH* chemiluminescence signal with passband from 1500 to 5000 Hz.

axis of the flame, fluctuations are zero as positive and negative contribution cancel when integrating along a line of sight.

The phase information of OH* chemiluminescence fluctuations is not shown here explicitly: The phase obtained from the Fourier transform of time series with regard to pressure readings does not depend on the location. The simultaneously with the OH* chemiluminescence recorded pressure signal – the pressure is recorded approximately at $x = 0$ mm and $y = 62$ mm – is in phase with the OH* chemiluminescence around a frequency of 3.3 kHz when evaluating the Fourier spectra. Fig. 13 shows a bandbass filtered time trace of pressure and OH* signal. The time series is bandpass filtered from 1500 to 5000 Hz, which does not remove any essential information when showing a modulation of the limit cycle amplitude. Bandpass filtering is mainly done to set the mean value for the pressure and the OH* chemiluminescence to zero to simplify reading. The interaction of OH* chemiluminescence and pressure is obvious: If OH* signal and pressure are in phase, pressure and OH* amplitudes grow as indicated by the Rayleigh criterion for thermoacoustic instabilities. If they are out of phase, pressure amplitudes start decaying until oscillations are in phase again. Here the authors would like to recall Fig. 5, in particular the secondary peaks related to a low-frequency modulation of the limit-cycle amplitude. The modulation of the amplitude originates from the interaction of heat release and acoustic pressure.

Feedback mechanism

Finally, a feedback mechanism leading to the HF thermoacoustic instability can be proposed. The mechanism is based on the observations presented above. The transverse acoustic mode in the flame tube triggers the vortex shedding at the inner corner of the front plate, i.e. the shear layer between the unburnt mixture and the outer recirculation zone, where the unburnt mixture enters the combustion chamber: The acoustic velocity deflects the flow of unburnt mixture. As the momentum of the unburnt mixture is high, the flow of unburnt mixture does not attach to the front plate directly when driven upwards. The terms upwards and downwards refer to the situation as depicted in Fig. 10. The flow separates at the corner, a small zone of recirculated combustion products is formed as the unburnt mixture attaches further up to the front plate, initiating the vortex generation.

The vortical structures containing combustion products are forced downwards, as soon as the direction of the acoustic velocity turns. The vortices are exposed to the flow of unburnt mixture. The vortices are then convectively transported with the unburnt mixture. From the evolution of the vortices seen in the Mie-scattering images and the position of maximum heat release fluctuations, it is presumed that impinging on the flame, these coherent structures are driving the fluctuating heat release rate which in turn amplifies the amplitude of the T1 mode. To strengthen this hypothesis PLIF will be used in the future to analyze the flame and, as in the present configuration the flame is not compact, local Rayleigh indices will be used to quantitatively estimate the thermoacoustic coupling strength [20, 21].

CONCLUSIONS

A self-excited transverse acoustic mode in a cylindrical combustion chamber is investigated. It is shown that the dominating first transverse mode is rotating. Mie-scattering images, recorded at a repetition rate of 20 kHz, show a periodic formation of pockets with combustion products in the unburnt mixture, which are convectively transported with the mean flow. Formation of pockets of combustion products and pressure oscillations are in phase. With PIV measurements the mechanism responsible for the formation of combustion product zones is illustrated. The acoustic fluctuation triggers the generation of vortices in the shear layer between burnt and unburnt mixture at the front plate, where the unburnt mixture enters the flame tube. The position of the core of the vortices coincides with the combustion product pockets. These vortices, convected forward, are interacting with the flame. The resulting coherent heat release fluctuations locally – as well as in an integral sense – satisfy the Rayleigh criterion leading to the growth of the acoustic oscillations until saturation leads to a stable limit cycle.

ACKNOWLEDGMENT

This work was financially supported by ALSTOM Power Systems GmbH, Mannheim, the Bavarian State Ministry of Sciences, Research and the Arts and the Bavarian State Ministry for Economic Affairs, Infrastructure, Transport and Technology within the framework of KW21. Financial support from the Bavarian State Ministries is granted within the ”Klimaprogramm Bayern 2020”.

REFERENCES

[1] Pankiewitz, C., and Sattelmayer, T., 2003. “Time domain simulation of combustion instabilities in annular combustors”. *Journal of Engineering for Gas Turbines and Power*, ***125***(3), pp. 677–685.

[2] Sattelmayer, T., and Polifke, W., 2003. “Assessment of methods for the computation of the linear stability of combustors”. *Combustion Science and Technology*, ***175***, pp. 453–476.

[3] Sattelmayer, T., and Polifke, W., 2003. “A novel method for the computation of the linear stability of combustors”. *Combustion Science and Technology*, ***175***, pp. 477–497.

[4] Paschereit, C. O., Gutmark, E., and Weisenstein, W., 1999. “Coherent structures in swirling flows and their role in acoustic combustion control”. *Physics of Fluids*, ***11***, pp. 2667–2678.

[5] O’Connor, J., Natarajan, S., Malanoski, M., and Lieuwen, T., 2010. “Disturbance field characteristics of a transversely excited annular jet”. In Proceedings of ASME Turbo Expo 2010.

[6] Huang, Y., Wang, S., and Yang, V., 2006. “Systematic analysis of lean-premixed swirl-stabilized combustion”. *AIAA Journal*, ***44***, pp. 724–740.

[7] Huang, Y., and Yang, V., 2009. “Dynamics and stability of lean-premixed swirl-stabilized combustion”. *Progress in Energy and Combustion Science*, ***35***, pp. 293–364.

[8] Thomson, W., 1871. “Hydrokinetic solutions and observations”. *Philosophical Magazine*, ***42***, pp. 362–377.

[9] von Helmholtz, H. L. F., 1868. “Über discontinuierliche Flüssigkeits-Bewegungen [On the discontinuous movements of fluids]”. *Monatsberichte der Königlichen Preussische Akademie der Wissenschaften zu Berlin [Monthly Reports of the Royal Prussian Academy of Philosophy in Berlin]*, ***23***, pp. 215–228.

[10] Sangl, J., Mayer, C., and Sattelmayer, T., 2010. “Dynamic adaptation of aerodynamic flame stabilization of a premix swirl burner to fuel reactivity using fuel momentum”. In Proceedings of ASME Turbo Expo 2010: Power for Land, Sea and Air.

[11] Gülder, O. L., Smallwood, G. J., Wong, R., Snelling, D. R., Smith, R., Deschamps, B. M., and Sautet, J.-C., 2000. “Flame front surface characteristics in turbulent premixed propane/air combustion”. *Combustion and Flame*, ***120***, pp. 407–416.

[12] Pfadler, S., Beyrau, F., and Leipertz, A., 2007. “Flame front detection and characterization using conditioned particle image velocimetry (cpiv)”. *Optics Express*, ***15***, pp. 15444–15456.

[13] Lauer, M., and Sattelmayer, T., 2008. “Heat release calculation in a turbulent swirl flame from laser and chemiluminescence measurements”. In 14th Int Symp on Applications of Laser Techniques to Fluid Mechanics.

[14] Winkler, A., Wäsle, J., and Sattelmayer, T., 2005. “Experimental investigations on the acoustic efficiency of premixed swirl stabilized flames”. In 11th AIAA/CEAS Aeroacoustics Conference (26th AIAA Aeroacoustics Conference).

[15] Rayleigh, J., 1945. *The theory of sound*, Vol. II. Dover Publications.

[16] Putnam, A., and Dennis, W., 1954. “Burner oscillations of the gauze-tone type”. *Journal of the Acoustical Society of American*, ***26***, pp. 716–725.

[17] Enflo, B. O., and Hedberg, C. M., 2002. *Theory of nonlinear acoustics in fluids*. Kluwer Academic Publishers.

[18] Harrje, D. T., and Reardon, F. H., 1972. *Liquid propellant rocket combustion instabilities*. NASA.

[19] Noiray, N., Bothien, M., and Schuermans, B., 2011. “Investigation of azimuthal staging concepts in annular gas turbines”. *Combustion Theory and Modeling*, ***In press***.

[20] Kang, D., Culick, F., and Ratner, A., 2007. “Combustion dynamics of a low-swirl combustor”. *Combustion and Flame*, ***151***, pp. 412–425.

[21] Martin, C. E., Benoit, L., Sommerer, Y., Nicoud, F., and Poinsot, T., 2006. “Large-eddy simulation and acoustic analysis of a swirled staged turbulent combustor”. *AIAA Journal*, ***4***, pp. 741–750.

